JOURNAL OF CATALYSIS 36, 224–234 (1975)

Molecular Beam Study of Formic Acid Decomposition on Platinum

S. C. DAHLBERG,[1] G. A. FISK[2] AND R. R. RYE[2]

Department of Chemistry and Materials Science Center, Cornell University, Ithaca, New York 14850

Received July 8, 1974

The decomposition of formic acid on polycrystalline platinum has been studied under conditions such that the reaction occurs as the result of a single collision of formic acid with the surface, and a direct line of sight exists between the platinum surface and the detector. Under our experimental conditions, the reaction is first order in formic acid, with CO_2 and H_2 as the main products (~85%) and the remainder CO and probably H_2O. At 1150 K there is an abrupt increase in the steady state activity, and after heating to above this temperature a transient high activity (super-activity) exists when the sample is cooled to lower temperatures. This transient superactivity decays inversely with time to the steady state reaction rate. To explain these phenomena a five step mechanism is proposed. Two of the steps involve dissociative adsorption on paired sites of a diatomic poison whose main effect is to decrease the number of surface sites available for formic acid decomposition. Desorption of this poison explains the increase in activity at 1150 K, and readsorption is shown to explain the time dependence of the decay of the superactivity. The poison is suspected to be oxygen, but evidence on this point is incomplete.

INTRODUCTION

During the past 10 yr, the molecular beams technique has been developed into a valuable tool for studying solid surfaces (*1–3*). Most surface molecular beam research has involved molecules which do not interact chemically with the surface. Recently, there has been increased interest in molecular beam/surface systems which involve chemical interactions. This work falls into two categories: corrosion and catalysis. In the case of corrosion (*4–10*), a chemical reaction occurs between the beam molecules and the solid surface, forming a stable product which either desorbs or becomes incorporated into the bulk. Our own interest is with the second category, catalysis. In this case, the solid surface does not form permanent chemical bonds with the incoming molecules. Instead, the chemical interaction with the solid surface is temporary and the solid surface functions as a catalyst for reactions of the beam material. Included in this second category are examples of exchange (*11*), addition (*12–14*), and decomposition (*16–19*).

We report here a molecular beam study of the decomposition of formic acid on polycrystalline Pt, a reaction well suited for molecular beam studies for a number of reasons. (1) The reaction has been studied using conventional catalytic techniques for a number of years. The review by Mars *et al.* (*19*) is an excellent summary of this information. (2) The reaction has been reported to have a relatively low activation energy of 6.2 kcal/mole (*20*) at low formic acid pressures; and therefore each collision has a substantial probability of leading

[1] Present address: Bell Telephone Laboratories, Inc., Murray Hill, NJ 07974.

[2] Present address: Sandia Laboratories, Albuquerque, NM 87115.

to decomposition. It should thus be an easy reaction to study using the molecular beam technique. (3) The likely reaction products, either CO and H_2O, or CO_2 and H_2, are simple and desorb readily from Pt. Both sets have been observed, with CO_2 and H_2 the predominant products on Pt as well as on other metals. (4) Despite the large amount of work which has been directed toward this relatively simple reaction, large gaps in understanding still remain. A major point in question is the nature of the superactivity phenomenon which results from flashing the catalyst to high temperatures (*21–23*). The decay of this superactivity is too fast to be studied adequately by conventional techniques. We have been able to show that this superactivity decays inversely with time under our experimental conditions, and arguments will be presented to show that this decay is due to the adsorption of a gas phase poison.

EXPERIMENTAL

The vacuum chamber was composed of a Pyrex glass cross (diameter = 20 cm, length = 46 cm) with 0-ring grooves in the end of each arm. The cross was sealed to the top flange of a gate valve below which was mounted a diffusion pump (NRC VHS-4). The diffusion pump was equipped with a liquid nitrogen cooled baffle (NRC 0316) and backed by a suitable mechanical pump. Cylindrical brass liquid nitrogen traps were attached to, but thermally insulated from, flanges which sealed the two horizontal openings of the cross. One of these cylindrical liquid nitrogen traps was designed so that a quadrupole mass spectrometer would fit along the trap axis. The cylindrical liquid nitrogen traps had extensions which surrounded the reaction zone, the center region of the cross. In this manner, the reaction zone was completely surrounded by liquid nitrogen cooled surfaces except for an opening into the diffusion pump and a small opening for target insertion. Pressure was measured in a small side arm located just above the baffle by means of a Bayard-Alpert ionization gauge. A base pressure of 3×10^{-7} Torr was obtained at the gauge with the molecular beam off. With the beam on, the pressure was typically 2×10^{-6} Torr. A flange carrying the molecular beam oven and a target mount assembly was placed in the top opening of the cross. Figure 1 is a schematic drawing which shows a cutaway top view of the reaction zone. A rectangular polycrystalline Pt foil was mounted in the center of the reaction zone with axes of both the oven and the mass spectrometer perpendicular to the long (vertical) dimension of the Pt target. The apparatus was designed so that the oven and target mount could be independently coaxially rotated from outside the vacuum chamber. In this manner, the angle of beam incidence and the angle of mass spectrometer detection relative to the target normal could be varied. This allowed angular distributions of the desorbed species to be studied. However, for the majority of the work reported here, the angle of beam incidence and mass spectrometer detection remained fixed at, respectively, 60 and 0° from the normal to the Pt surface.

A thermal formic acid beam was obtained by using the vapor over liquid formic acid (Matheson, Coleman and Bell) held at room temperature. The formic acid flux was regulated with a needle valve. The molecular beam oven consisted of a small box with a slit (.062 mm wide, 1 cm long); it was maintained at room temperature by resistance heating of overwound nichrome wire. Cold slits were placed in front of the oven to collimate the molecular beam. In addition to collimation of the source, liquid nitrogen cooled slits were placed between the Pt foil and the mass spectrometer to discriminate strongly in favor of those products which came directly from the foil.

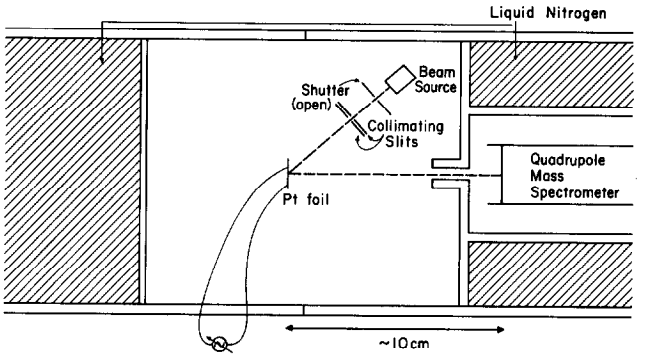

FIG. 1. Schematic drawing showing the molecular beam reaction zone.

Polycrystalline Pt foil (0.25 mm thick, 3 cm length, 1 cm wide; Fisher Scientific Co.) was spotwelded between spring loaded molybdenum rods (.31 cm diameter) to keep the Pt foil flat during thermal expansion. The Pt was resistively heated and its temperature was monitored using a W-5% Re/W-26% Re thermocouple spotwelded to the back of the Pt foil. At high temperatures, the thermocouple measurements agreed to within ±5 K with the temperature measured using an optical pyrometer ($\epsilon_{Pt} = 0.30$).

Before each day's work, the Pt was subjected to an oxidation procedure similar to the cleaning treatments (checked in some cases by Auger spectroscopy) reported by several workers (*24–27*). The foil was held at 1470 K in 6×10^{-5} Torr O_2 for 15 min. This procedure gave reproducible, catalytically active surfaces.

The loss of formic acid and the gain of decomposition products were measured using a quadrupole mass spectrometer (Granville Phillips Spectrascan 400 Residual Gas Analyzer). In all cases, the mass number chosen to represent the species was the parent number (e.g., formic acid = mass 46). The mass spectrometer output was measured on a high speed picoammeter with current suppression capability. This signal and the thermocouple emf were recorded on a two pen strip chart recorder.

In order to separate that part of a mass spectrometer signal due to formic acid decomposition from that due to background gases, a shutter operated from outside the vacuum chamber was placed in front of the formic acid oven. With the shutter closed, little formic acid could impinge on the Pt and the background mass spectrometer signal was measured. With the shutter open, formic acid impinged directly onto the Pt and the mass spectrometer signal, which included both the background and the decomposition contributions, was again measured. The reported measurement is in all cases the shutter open–shutter closed difference signal.

To account for differences in pumping speeds and mass spectrometer sensitivities for different species, the mass spectrometer was calibrated with measured fluxes of CO_2, CO, and H_2 under conditions approximating as closely as possible the experimental conditions of the molecular beam work. In order to simulate material leaving the Pt foil, the target mount was removed and a small oven was placed in the same position as the Pt foil. This oven was designed so that molecules leaving it would have a cosine distribution. Connected to this oven through a needle valve was a large glass bulb ($V_B \approx 1$ liter). The pressure in this bulb was measured using a McLeod gauge. The bulb was filled with the gas to be studied at a pressure of 1 Torr. With the needle valve closed, the background mass spectrometer signal at the appropriate mass number was mea-

sured. The needle was then opened and a new signal was established in the vacuum chamber. As the bulb emptied, both the bulb pressure and the mass spectrometer signal were measured as functions of time. The mass spectrometer signal (subtracting the background) was linearly dependent on the sample bulb pressure over the entire pressure range studied.

The calibration analysis is straightforward. The flux of molecules out of the sample bulb is given by $V_B(dB_B/dt)$, and in the pressure range of interest the flux through an orifice is proportional to the pressure difference across the orifice (*28*). In our case this is the difference between the sample bulb and vacuum system pressures, $P_B - P_{VS}$. Thus we can write:

$$-V_B(dP_B/dt) = F(P_B - P_{VS}) \approx F(P_B). \quad (1)$$

The proportionality constant, F, is a constant for each gas and the effective orifice includes the pinhole, needle valve and connecting tubing. F is obtained from the time dependence of the sample bulb pressure. Since the mass spectrometer signal is experimentally observed to vary linearly with the sample bulb pressure and the flux out of the oven is proportional to the bulb pressure, the relationship between the mass spectrometer signal, i, and flux can be expressed as

$$F(P_B) = \beta i = \text{input flux}. \quad (2)$$

With F previously determined as above, the calibration factor, β, is obtained from the slope of a plot of sample bulb pressure vs signal. Since the calibration oven is designed so that the flux from the oven duplicates as closely as possible the flux from the target, the value of β so obtained is valid for a flux of material leaving the target. In order to have a more accurate measure of the relative amounts of the various products, we have used ratios of the calibration factors (e.g., β_{CO}/β_{H_2}) in order to take advantage of cancellation of factors, such as the volume of the sample bulb, which could introduce errors. Moreover, our inability to obtain a calibration for formic acid, due to condensation in the McLeod gauge, eliminates the usefulness of an absolute calibration.

RESULTS AND INTERPRETATION

When a molecular beam of formic acid impinges on a polycrystalline Pt target, the decomposition products we observe are CO_2, H_2, and CO. Figure 2 shows the steady state signals for the rate of formation of these decomposition products and the rate of loss of formic acid reactant as functions of the "flux" of formic acid for a surface temperature of 1400 K. For the products, the recorded mass spectrometer signals have been corrected for the con-

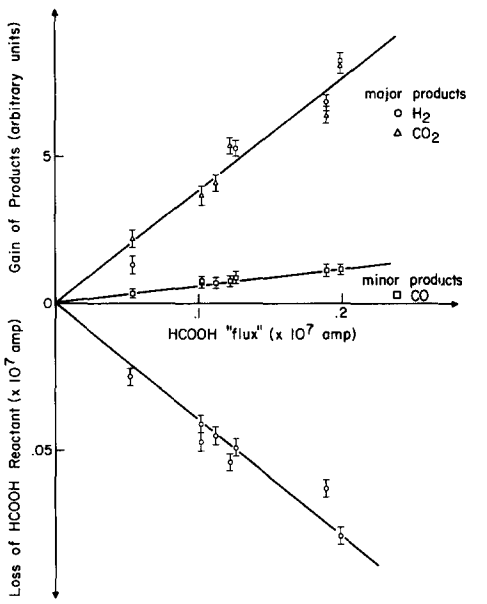

FIG. 2. Gain of products and loss of reactant vs formic acid "flux" at 1400 K. The gain of a product is the mass spectrometer signal corrected for fragmentation of formic acid and scaled by the internally consistent calibration factor. The loss of formic acid is the difference between the signal at 1400 K and that with the target cold. Each point is the average of a series of identical measurements with experimental scatter given by the error bars. The "flux" of formic acid (proportional to the actual incident flux) is the mass spectrometer signal of formic acid reflected from an inactive, cold (250 K) surface.

tribution from fragmentation of formic acid in the mass spectrometer, and the results scaled using the relative calibration factors. The "flux" is proportional to the actual flux of formic acid onto the target and is obtained by measuring the formic acid signal reflected from a cold (250 K) surface; at this temperature no measurable difference signals are observed other than those from fragmentation of formic acid in the mass spectrometer. Comparison of the calibrated mass spectrometer signals shows that H_2 and CO_2, produced in equal amounts, are the major decomposition products. There is also a CO product signal about 15% as large as those of the major products. From stoichiometry, we expect H_2O also to be a minor product. Because of the large mass 18 signal from fragmentation of formic acid in the mass spectrometer, however, a H_2O signal of magnitude corresponding to the CO would be very difficult to detect experimentally (signal/noise ≤ 0.2), and no H_2O data were obtained under these conditions.

The angular distributions of scattered formic acid and the decomposition products have been determined for surface temperatures of 730 and 1270 K. For both H_2 and CO the signals are independent of angle, while for CO_2 and HCOOH the distributions are approximately cosine relative to the target normal. This difference is most probably due to different effective pumping speeds for the two sets of molecules on the liquid nitrogen cooled walls. H_2 and CO are not condensable under our operating conditions, and have pumping constants determined predominantly by the diffusion pump. In our apparatus molecular velocities and the dimensions of the reactor are such that randomization occurs within the residence time of a molecule in the reactor. CO_2 and especially HCOOH are condensable and the walls act as a very effective additional pump. For these species, randomization does not occur, and the observed angular dependence of the signal yields directly the probability that a molecule leaves the surface at a given angle. The scattering distribution for formic acid is most probably an example of trapping-dominated scattering as discussed by Weinberg and Merrill (*29*). Such scattering, characterized by a $\cos\theta$ component, is expected when the well depth, D, is greater than twice the average kinetic energy of a molecule impinging from the gas phase (*30*). The adsorption of formic acid on platinum should be characterized by a deep well, and the foregoing inequality satisfied for our conditions. Hence, cosine scattering is to be expected. It might also be possible that a component of this cosine distribution is due to scattering from a surface coverage of light atoms arising from adsorption from either the beam or the background. Such cosine scattering has been observed by West and Somorjai for C_2H_2 from an C_2H_2 covered surface and for CO from a CO covered surface (*31*). However, since we observe the same scattering distributions at 730 and at 1270 K, where later arguments and evidence indicate that the surface is relatively free of adsorbed atoms or molecules, such an effect is apparently negligible in our experiments.

Figure 2 shows that the decomposition product signals are linear in formic acid flux. A previously proposed (*19*) three step mechanism is adequate for explanation of this observed linear behavior:

$$\mathrm{HCOOH} + * \underset{k_{-1}}{\overset{k_1}{\rightleftharpoons}} \underset{*}{\mathrm{HCOOH}}, \qquad (3a)$$

$$\underset{*}{\mathrm{HCOOH}} \xrightarrow{k_2} \mathrm{CO_2} + \mathrm{H_2} + *, \qquad (3b)$$

$$\underset{*}{\mathrm{HCOOH}} \xrightarrow{k_3} \mathrm{CO} + \mathrm{H_2O} + *. \qquad (3c)$$

The notation * represents an empty Pt surface site, and HCOOH represents a Pt surface site occupied by formic acid. CO_2, CO, H_2O, H_2 and HCOOH are gas phase species. Modifications to this mechanism will be presented later in this paper. Under the experimental conditions employed to

collect the data presented in Fig. 2, a steady state concentration of formic acid is established on the surface; the mechanism of Eq. (3) then gives

$$\frac{d(\underset{*}{\text{HCOOH}})}{dt} = 0 = k_1(\text{HCOOH})(*) - (k_{-1} + k_2 + k_3)(\underset{*}{\text{HCOOH}}). \quad (4)$$

This mechanism contains an additional constraint in that the total number of sites, N, is a constant.

$$N = (*) + (\underset{*}{\text{HCOOH}}). \quad (5)$$

By using Eqs. (4) and (5), we can write the rate equations for the steady state production of H_2 or CO_2:

$$\frac{d(H_2)}{dt} = \frac{d(CO_2)}{dt} = \frac{k_2 k_1(\text{HCOOH})}{k_{-1} + k_2 + k_3} \cdot \frac{N}{1 + [k_1(\text{HCOOH})/(k_{-1} + k_2 + k_3)]}. \quad (6)$$

The rate expression for H_2O or CO is obtained from Eq. (6) by substitution of k_3 for k_2 in the numerator. Experimentally, the rates are proportional to the mass spectrometer signals (e.g., $d(H_2)/dt \propto i_{H+2}$). This is a familiar Langmuir–Hinshelwood type kinetic rate law (*32*) for which there are two limiting cases. At low formic acid fluxes, $1 \gg k_1(\text{HCOOH})/(k_{-1} + k_2 + k_3)$, the decomposition will have first order dependence on formic acid flux, as we observe. This corresponds to very low surface coverages of formic acid, as can be seen using Eq. (4). The second limiting case occurs at large formic acid fluxes, where the previous inequality is reversed. In this case the decomposition will have zero order dependence on the formic acid flux. This corresponds to surface coverages of formic acid approaching unity. Both limiting formic acid dependences have been reported in the literature, with transition from first to zero order occurring at pressures corresponding to impact rates of $\sim 3 \times 10^{20}$ molecules cm^{-2} sec^{-1} (*33*). Under our experimental conditions (formic acid flux estimated to be $\sim 3 \times 10^{15}$ molecules cm^{-2} sec^{-1}), first order behavior is always observed.

Figure 3 shows detected signals as functions of the Pt temperature. The axis marked "gain of products" and "loss of reactants" is the calibrated shutter open minus shutter closed mass spectrometer difference signal. This is proportional to the rate of product production or to the rate of reactant consumption. The closed symbols are steady state measurements. The open symbols are non-steady state values obtained in the following manner. The foil was heated to a temperature greater than 1150 K and held at this temperature for 10 min. The temperature dependence of the signals was then recorded as the target cooled rapidly (~ 550 K/min).

Consider first the steady state case. From the data in Fig. 3, we can obtain the ratio of major to minor products as a function of the temperature of the Pt; this is

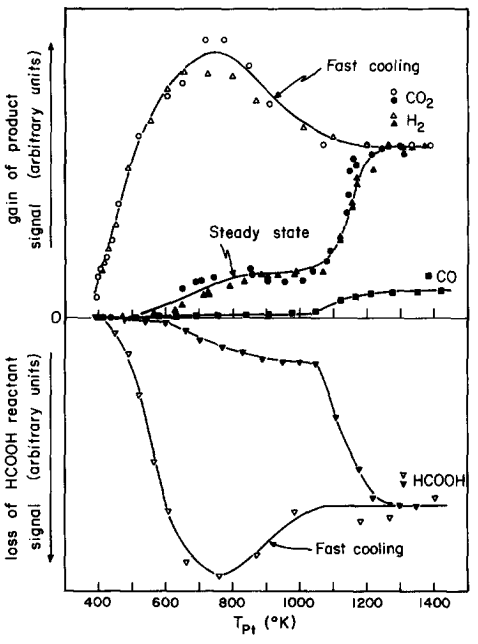

FIG. 3. Temperature dependence of formic acid decomposition. The ordinate is the same as in Fig. 2. Closed symbols are steady state data points and open symbols are data resulting from heating to $T > 1150$ K followed by rapid cooling to lower temperatures.

shown in Fig. 4. According to the proposed mechanism, this ratio is just k_3/k_2. All decomposition product signals and the loss of formic acid show sharp increases at 1150 K. At this temperature, the decomposition rate increases by a factor of ~5, but there is no anomaly in the CO/CO_2 ratio at this temperature (Fig. 4). This suggests that the decomposition mechanism is not changing near 1150 K, a point which will be dealt with in more detail later.

The non-steady state behavior given by the open symbols in Fig. 3 is somewhat more complicated than the steady state behavior. To obtain this behavior the Pt must be activated by heating to temperatures exceeding 1150 K. After this activation, the catalytic activity during cooling is transiently much larger than the steady state activity for Pt temperatures less than 1150 K. If the Pt target is cooled to a fixed temperature instead of being continuously cooled over a range of temperatures, this superactivity is observed to decay to the steady state activity over a period of several minutes. Temperatures near 1150 K

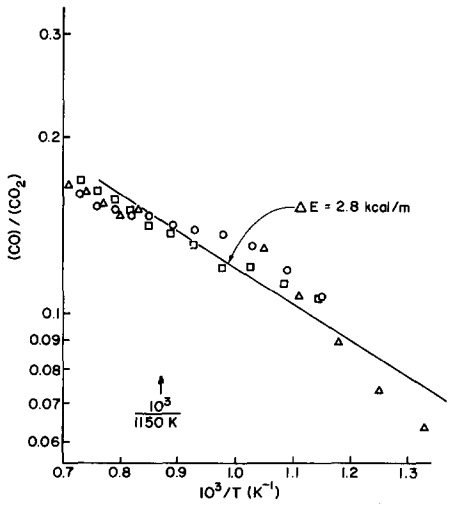

FIG. 4. Temperature dependence of the ratio of minor to major products at steady state. The arrow indicates the temperature at which the break occurs in the steady state activity shown in Fig. 3. Different symbols refer to different runs.

are thus associated with both the abrupt increase in the steady state activity and the activation process; heating the target to temperatures less than 1150 K yields no enhanced activity when the target is subsequently cooled. The superactivity of recently flashed metals has been reported in the literature for a variety of metals and reactions (*34,35*), including formic acid decomposition (*21–23*). In our work, activation occurs regardless of whether formic acid is allowed to impinge on the surface during the activating treatment. We find that the rate of activation depends on the recent thermal history of the target. If the target has been left cold for several hours, activation is not immediate upon heating; the target must be heated to above 1150 K for several minutes before the hydrogen signal reaches its full value. However, if a recently activated target is deactivated and again flashed to above 1150 K, reactivation is immediate.

The initial superactive signal and the decay of the superactivity as a function of time at fixed Pt temperature are the same for both CO_2 and H_2. To represent the time dependence of the decay, several functional forms were investigated. Figure 5 shows, for the H_2 product signal, the form which best fits the experimental data: a plot of the reciprocal of the hydrogen signal vs time. It should be remembered that the hydrogen signal is proportional to the rate of production of hydrogen. Before collecting the data shown in Fig. 5, the Pt was activated at 1400 K. All the data in Fig. 5 have been normalized by dividing by the 1400 K steady state H_2 signal. Both the slopes and the intercepts of the data depend on the temperature of the Pt. The slope, or rate of decay of the superactivity, increases with decreasing temperature, and the intercept, the reciprocal of the initial amount of superactivity at time zero, decreases with decreasing temperature. In other words, there is both increased superactivity and increased rate of superactivity decay as the temperature is de-

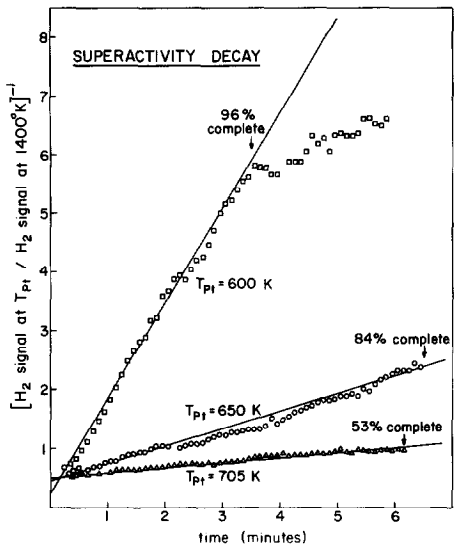

FIG. 5. Decay of the superactive H_2 signal as a function of time. The reciprocal of the H_2 signal has been normalized to that at 1400 K, and the arrows indicate the percentage completion of decay at the indicated time.

creased. The competition between these two effects leads to the apparent maximum in the superactivity data presented in Fig. 3.

All three observable decomposition products and the loss of formic acid reactant show the superactivity phenomena. Both during the superactivity decay at a fixed temperature (Fig. 5) and during the fast cooling over a range of temperatures (Fig. 3), the loss of formic acid is found to parallel the gain of the major decomposition products. This indicates that the time required for establishment of a steady state reaction condition for formic acid decomposition (Equation (4)) is short compared to the decay time of the superactivity. The decay of the superactivity is also found to be independent of HCOOH flux onto the surface and independent of addition of decomposition products in the gas phase.

DISCUSSION

The three step mechanism given by Eq. (3) is capable of explaining several aspects of the formic acid decomposition. However, this oversimplified mechanism cannot explain the observed characteristic break temperature at 1150 K and the transient superactivity. A modification is suggested by the form of the time dependence of the superactivity decay. The inverse dependence of product production rate on time is consistent with dissociative chemisorption of a gas phase poison requiring two adjacent surface sites (*36*). Previous models for superactivity have involved bulk diffusion of either carbon or vacancies (*23*). These bulk diffusion models fail to predict the correct time dependence for the decay of superactivity. As a result of later analysis of the temperature dependence of the poisoning step, we assume that adsorption of the poison initially goes through a precursor state, and propose the following modifications to the mechanism of Eq. (3):

$$X_2 \underset{k_{-4}}{\overset{k_4}{\rightleftharpoons}} (X_2)_{ads.} \quad \text{(fast)}, \tag{7}$$

$$2 * + (X_2)_{ads.} \underset{k_{-5}}{\overset{k_5}{\rightleftharpoons}} 2\underset{*}{X}. \tag{8}$$

Desorption of this poison would explain the existence of the characteristic break temperature seen both in the activation of the superactivity and in the abrupt increase in the steady state activity. Comparison of this break temperature with the desorption temperatures of possible gas phase poisons suggests oxygen (*37–39*) as the most likely candidate for the poison; but, as discussed later, evidence on this point is incomplete. Thus, we use here the noncommittal notation of X_2 for the poison.

First consider the effect of adding the additional steps represented by Eqs. (7) and (8) to the simple three step mechanism. The expression for the constraint on the total number of surface sites (Eq. (5)) must now be modified to include the number of sites used by the poison:

$$N = (*) + (\underset{*}{HCOOH}) + (\underset{*}{X}). \tag{9}$$

In the limit that the reaction given by Eq. (7) is fast enough to come to equilibrium,

the expression for the steady state rate of production of H_2 or CO_2 is

$$\frac{d(H_2)}{dt} = \frac{d(CO_2)}{dt} = \frac{k_2 k_1 (HCOOH)}{(k_{-1} + k_2 + k_3)} \frac{N}{1 + [k_5 k_4 (X_2)/k_{-5} k_{-4}]^{1/2} + [k_1 (HCOOH)/(k_1 + k_2 + k_3)]}. \quad (10)$$

As was the case for the original mechanism, the rate of production of CO or H_2O is obtained from Eq. (10) by replacing k_2 with k_3 in the numerator. The modified mechanism also still predicts first order dependence on formic acid for small formic acid fluxes, and zero order dependence on formic acid for large fluxes. In these respects, the original and modified mechanisms make the same predictions, with the modification that the poisoning step reduces the decomposition rate due to blocking of surface sites.

If the poison is removed by heating the Pt to high temperatures, the new mechanism predicts that, initially, the surface should be relatively free of poison and highly active when cooled to lower temperatures, as is seen experimentally. This high activity is not permanent. Poison readsorbs on the surface and the high activity decays to the steady state activity with observed decay times which are reasonable given realistic values for sticking coefficient and background pressure of the poison. A quantitative prediction of the rate of superactivity decay using the modified mechanism proceeds as follows. Since our experimental conditions are such that the decomposition rate is first order in formic acid, the formic acid term in Eq. (9) can be neglected. We then can write, using Eqs. (7) and (8), for a constant pressure of poison,

$$\frac{d(\underset{*}{X})}{dt} \approx \frac{2k_5 k_4 (X_2)}{k_{-4}} [N - (\underset{*}{X})]^2 - 2k_{-5} (\underset{*}{X})^2. \quad (11)$$

During the initial decay, the step involving k_{-5} has a negligible rate compared to the forward step. Neglecting this term and integrating yields:

$$\frac{1}{(*)} \approx \frac{1}{[N - (\underset{*}{X})]} \approx \frac{2k_5 k_4}{k_{-4}} (X_2) t + \frac{1}{N}. \quad (12)$$

The integration constant $1/N$ is obtained by assuming that after the activation at 1400 K, the poison has essentially zero coverage on the Pt surface. Because the decomposition rate is directly proportional to the concentration of adsorbed formic acid and because this in turn is directly proportional to the concentration of free sites (Eq. (4), steady state constraint on formic acid), the decomposition rate during the initial super activity decay is

$$\left[\frac{d(H_2)}{dt}\right]^{-1} = \left[\frac{d(CO_2)}{dt}\right]^{-1} \frac{k_{-1} + k_2 + k_3}{k_2 k_1 (HCOOH)} \left[\frac{2k_5 k_4}{k_{-4}} (X_2) t + \frac{1}{N}\right]. \quad (13)$$

The initial transient rates of production of CO and H_2O follow on replacing k_2 with k_3 in the denominator of the first term in Eq. (13). Equation (13) is written in the reciprocal form in order to show its agreement with the form observed experimentally (Fig. 5). This equation is also in agreement with experiment in that CO_2 and H_2 have the same initial superactivity and the same rate of decay. The fact that the experimental data are linear over much of the decay implies that neglect of the desorption term in Eq. (11) is valid to very high coverages of poison. According to Eq. (13), the decay also depends linearly on the concentration of the poison, (X_2). We have shown that neither the reactant nor any of the observed products has an effect on the rate of decay of superactivity; they can thus be eliminated from consideration

as the poison. The effect of oxygen is more complex and is not yet fully understood. Deliberate addition of oxygen to the gas phase in order to check its effect on the decay rate is complicated by its modification of the steady state reaction: Large measurable quantities of water are produced, and the shape of the hydrogen signal vs temperature is changed.

Experimentally, both the slopes and the intercepts in Fig. 5 are temperature dependent, an observation in agreement with Eq. (13) in which the temperature dependence is carried in the individual rate constants. According to Eq. (13), the intercepts plotted in Fig. 5 are given by

$$\frac{[(k_{-4}+k_2+k_3)/k_2k_1]_T}{[(k_{-1}+k_2+k_3)/k_2k_1]_{1400\,\mathrm{K}}} \propto \exp\left[-\frac{E_i}{RT}\right]. \quad (14)$$

The overall activation energy, E_i, is observed experimentally to be 3.9 kcal/mole. Similarly, the slopes in Fig. 5 are given by

$$\frac{[(k_{-1}+k_2+k_3)/k_2k_1]_T}{[(k_{-1}+k_2+k_3)/k_2k_1]_{1400\,\mathrm{K}}} \frac{2(k_5k_4/k_{-4})_T(\mathrm{X}_2)}{1/N} \propto \exp\left[-\frac{E_s}{RT}\right] \quad (15)$$

and are characterized by an overall experimental activation energy, E_s, of -8.9 kcal/mole. The term in the denominator in each case is due to the normalization of the experimental data to the decomposition rate at 1400 K. Dividing Eq. (15) by (14) leads to

$$2\left[\frac{k_5k_4}{k_{-4}}\right]_T N(\mathrm{X}_2) \propto \exp\left[-\frac{(E_s-E_i)}{RT}\right]. \quad (16)$$

Without the precursor step for adsorption of the poison, Eq. (16) would contain only k_5 as a temperature dependent term and, from the values of E_s and E_i, there would be an unreasonable activation energy for direct adsorption of -12.8 kcal/mole. Inclusion of the precursor step leads to more reasonable values. Adsorption steps in general are at most weakly activated; therefore, we assume k_5 and k_4 to have no temperature dependence. This leaves k_{-4} as the only activated factor and yields an activation energy for desorption from the precursor state of approximately 12.8 kcal/mole. Oxygen, a likely poison, is reported to have a molecular binding state with adsorption energy in the range 5–15 kcal/mole (*38,39*).

Of the possible gas phase poisons, oxygen is the most likely. Other possible candidates such as H_2, CO, N_2, etc., are either not adsorbed on Pt or desorb at much lower temperatures than that observed for the break. In addition, with oxygen there is the possibility of forming a platinum oxide (*27,40–43*) which can act as a reservoir of surface poison and thus explain the time required for complete activation when the target has sat cold for several hours. The existence of such a platinum oxide is supported by preliminary analysis of our samples by ion probe mass spectrometry, which showed roughly a factor of 3 increase in the oxygen in the top 150 Å after use in the vacuum system. Lewis and Gomer (*43*) report large changes in their Pt field emission patterns as the temperature is varied in the range 1000–1200 K, the same temperature range in which we observe a large change in the formic acid decomposition rate. They interpret their results to indicate that Pt surface oxide and impurity metal surface oxides are decomposing in this temperature range.

Formic acid decomposition on platinum, in conditions other than ultra-high vacuum, is obviously more complicated than suggested by the previously proposed three step mechanism. The involvement of surface platinum oxide in this reaction, which is suggested by the time required for activation when the platinum target has been cold for several hours, would indicate that the reaction is even more complicated than is suggested by our modifications to

the mechanism. Further investigation of this point will require the use of techniques which are sensitive to surface and bulk compositions.

ACKNOWLEDGMENTS

The authors are indebted to Professor G. H. Morrison for obtaining the preliminary Ion Probe Mass Spectroscopy data on the oxygen content. This work was supported in part by the Department of Chemistry, and in part by NSF and ARPA through the Cornell Materials Science Center. One of us (S.C.D.) was supported by a NSF Traineeship during part of this work.

REFERENCES

1. SALTSBURG, H., *Ann. Rev. Phys. Chem.* **24,** 493 (1973).
2. SMITH, J. N., *Surface Sci.* **34,** 613 (1973).
3. SOMORJAI, G. A., "Structure and Chemistry of Solid Surfaces," 1st ed., John Wiley and Sons, New York, 1969.
4. OLANDER, D. R., JONES, R. H., SCHWARZ, J. A., AND SIEKHAUS, W. J., *J. Chem. Phys.* **57,** 408 (1972); **57,** 421 (1972).
5. MADIX, R. J., AND SCHWARZ, J. A., *Surface Sci.* **24,** 264 (1971); **24,** 288 (1971).
6. MCKINLEY, J. D., *J. Chem. Phys.* **40,** 120 (1964).
7. SMITH, J. N., AND FITE, W. L., *in* "Third International Symposium on Rarefied Gas Dynamics" (J. A. Lauramann, Ed.), p. 430. Academic Press, New York, 1963.
8. ANDERSON, J., AND BOUDART, M., *J. Catal.* **3,** 216 (1964).
9. MADIX, R. J., AND BOUDART, M., *J. Catal.* **7,** 240 (1967).
10. MADIX, R. J., AND SASU, A. A., *Surface Sci.* **20,** 377 (1970).
11. BERNASEK, S. L., SIEKHAUS, W. J., AND SOMORJAI, G. A., *Phys. Rev. Letters* **30,** 1202 (1973).
12. SMITH, J. N., AND PALMER, R. L., *J. Chem. Phys.* **56,** 13 (1972).
13. NUTT, C. W., AND KAPUR, S., *Nature (London)* **220,** 697 (1968).
14. SMITH, J. N., PALMER, R. L., AND VROOM, D. A., *J. Vac. Sci. Technol.* **10,** 373 (1973).
15. COLTHARP, R. N., SCOTT, J. T., AND MUSCHLITZ, E. E., JR., *J. Chem. Phys.* **51,** 5180 (1969).
16. WEST, L. A., AND SOMORJAI, G. A., *J. Vac. Sci. Technol.* **9,** 668 (1972).
17. SMITH, J. N., JR., AND FITE, W. L., *J. Chem. Phys.* **37,** 898 (1962).
18. KRAKOWSKI, R. A., AND OLANDER, D. R., *J. Chem. Phys.* **49,** 5027 (1968).
19. MARS, P., SCHOLTEN, J. J. F., AND ZWIETERING, P., *Advan. Catal.* **14,** 35 (1963).
20. BLOCK, J., AND VOGL, J., *Z. Elektrochem. Angew. Phys. Chem.* **63,** 3 (1959).
21. DUELL, M. J., AND ROBERTSON, A. J. B., *Trans. Faraday Soc.* **57,** 1416 (1961).
22. WILLHOFT, E. M. A., AND ROBERTSON, A. J. B., *J. Catal.* **9,** 358 (1967).
23. ROBERTSON, A. J. B., *in* "Chemisorption and Catalysis" (Peter Hupple, Ed.), p. 72. Elsevier, Amsterdam, 1970.
24. PIGNET, T. P., SCHMIDT, L. D., AND JARVIS, N. L., *J. Catal.* **31,** 145 (1973).
25. LAMBERT, R. M., WEINBERG, W. H., COMXIE, C. M., AND LINNETT, J. W., *Surface Sci.* **27,** 653 (1971).
26. MORGAN, A. E., AND SOMORJAI, G. A., *Surface Sci.* **12,** 405 (1968).
27. LANG, B., JOYNER, R. W., AND SOMORJAI, G. A., *Surface Sci.* **30,** 454 (1972).
28. DUSHMAN, S., *in* "Scientific Foundations of Vacuum Technique" (J. M. Lafferty, Ed.), p. 90. John Wiley and Sons, Inc., New York, London, Sydney, 1962.
29. WEINBERG, W. H., AND MERRILL, R. P., *J. Chem. Phys.* **56,** 2881 (1972).
30. SAU, R., AND MERRILL, R. P., *Surface Sci.* **34,** 268 (1973).
31. WEST, L. A., AND SOMORJAI, G. A., *J. Chem. Phys.* **57,** 5143 (1972).
32. LAIDLER, K. J., "Chemical Kinetics," p. 153. McGraw Hill Book Co., Inc., New York, Toronto, London, 1950.
33. FUKUDA, K., OHISHI, T., AND TAMARU, K., *Bull. Chem. Soc. Jap.* **42,** 1192 (1969).
34. ROBERTSON, A. J. B., AND WILLHOFT, E. M. A., *Trans. Faraday Soc.* **63,** 476 (1967).
35. LE GOFF, P., AND LETORT, M., *J. Chim. Phys.* **53,** 480 (1956); **54,** 3 (1957).
36. HAYWARD, D. D., AND TRAPNELL, B. M. W., "Chemisorption," 2nd ed., p. 90. Butterworths, London, 1964.
37. NISHIYAMA, Y., AND WISE, H., *J. Catal.* **32,** 50 (1974).
38. PROCOP, M., AND VOLTER, J., *Z. Phys. Chem. Leipzig* **250,** 387 (1972).
39. FUSY, J., EHRHARDT, J. J., AND CASSUTO, A., "Structure et Proprietes des Surfaces Solides," Colloques Internationaux du Centre de la Recherche Scientifique, no. 187, p. 163, 1970.
40. MELMED, A. J., *J. Appl. Phys.* **36,** 3691 (1965).
41. NORMAN, J. H., STALEY, H. G., AND BELL, W. E., *J. Phys. Chem.* **71,** 3686 (1967).
42. WOOD, B. J., ENDOW, N., AND WISE, H., *J. Catal.* **18,** 70 (1970).
43. LEWIS, R., AND GOMER, R., *Surface Sci.* **12,** 157 (1968).